NSOM Investigations of the Spectroscopy and Morphology of Self-Assembled Multilayered Thin Films

Josef Kerimo, David M. Adams, and Paul F. Barbara*

Department of Chemistry, University of Minnesota, 207 Pleasant Street Southeast, Minneapolis, Minnesota 55455

David M. Kaschak and Thomas E. Mallouk*

Department of Chemistry, The Pennsylvania State University, University Park, Pennsylvania 16802

Received: May 1, 1998; In Final Form: September 1, 1998

Near-field scanning optical microscopy (NSOM) and atomic force microscopy (AFM) have been employed to spatially resolve the complex nanoscale morphologies, spectroscopy, and energy-transfer efficiencies of self-assembled multilayered structures composed of alternating layers of α-zirconium phosphate [α-$Zr(HPO_4)_2$] (ZrP) and dye-labeled poly(allylamine hydrochloride) (dye-PAH) (where dye = Fluorescein (FL), Rhodamine B (RhB), or Texas Red (TR)). Two types of multilayer films have been investigated, namely, glass/anchor/ZrP/dye-PAH and glass/anchor/ZrP/dye-PAH/ZrP/dye-PAH, which were formed by the sequential layer-by-layer adsorption of the charged polyelectrolyte component layers. High- and low-coverage films were investigated. The glass/anchor/ZrP assemblies were shown to consist of a densely packed "tiled" motif of ZrP sheets which lie flat on the surface and cover more than 95% of the area, with average plate sizes of height = 13 (7) Å, width ≈ 150 nm. The dye-labeled polymer layers in glass/anchor/ZrP/dye-PAH and glass/anchor/ZrP/dye-PAH/ZrP/dye-PAH were shown to adhere to the surface of the ZrP sheets and fill in the cracks between the sheets to a lesser extent. The measured heights of these polymer-coated multilayer films are 26(9) and 48(15) Å, respectively. These heights are consistent with theoretical estimates of ideally packed ionic films (28 and 48 Å, respectively). Dual-wavelength fluorescence NSOM imaging at 580 nm and >610 nm and near-field photobleach experiments were used to spatially resolve nanoscopic regions that display energy transfer between the layers.

Introduction

There is considerable interest in the development of methods for the *molecularly controlled* assembly of nanostructured multilayered thin film materials.[1−8] One particularly promising type of multilayered thin film material is metal−phosphate and/or metal−phosphonate assemblies, which incorporate electrostatic, covalent, and/or coordinate interactions as the driving force for self-assembly. Such films have been designed, constructed, and in some cases tuned for photonic, electronic, and sensor applications.[5,9−16] Much of the current understanding of these materials has resulted from bulk analysis techniques (i.e., ellipsometry, X-ray diffraction, optical spectroscopy, X-ray photoelectron spectroscopy, and NMR spectroscopy) which provide information (i.e., film thickness, interlayer spacings, structure, and elemental content, etc.) that is averaged over macroscopic distances. The ability to monitor the self-assembly process at the nanoscopic and mesoscopic level, however, is essential for the future refinement of the synthesis, processing, and fabrication. High-resolution surface analysis microscopies such as atomic force microscopy (AFM) and scanning and transmission electron microscopy (SEM and TEM) have rarely been used to elucidate the morphologies of these films and additionally lack the chemical sensitivity to effectively determine the structure in some cases.[15−18]

This paper is focused on the morphological investigation of zirconium phosphate multilayer films prepared by self-assembly involving the sequential layer-by-layer adsorption of oppositely charged polyelectrolyte species.[9] Multilayer films in this process are formed in a simple dipping procedure in which a substrate is exposed sequentially to solutions containing oppositely charged polyelectrolytes. In principle, there are no restrictions to the substrate size and topology that can be modified with this technique, in contrast to the Langmuir−Blodgett technique which requires planar substrates. Using this layer-by-layer adsorption process, multilayer structures have been fabricated based on a motif of alternating layers of polyanionic α-zirconium phosphate [α-$Zr(HPO_4)_2$] (ZrP) and polycationic dye-derivatized poly(allylamine hydrochloride) (dye-PAH).[10] The molecular structure of the various polyelectrolyte components and the self-assembly procedure are displayed in Figure 1. The buildup of a typical layered structure begins with derivatization of a glass surface with (4-aminobutyl)dimethylmethoxysilane and subsequent protonation of the amine in water to yield a positively charged surface (denoted glass/anchor). Dipping of the amine-modified surface into a solution containing suspended polyanionic layers of ZrP results in the formation of a film of ZrP sheets electrostatically bound to the surface (glass/anchor/ZrP). Dipping of the polyanionic glass/anchor/ZrP surface into a solution containing polycationic dye-PAH yields the multilayer structure glass/anchor/ZrP/dye-PAH. More layers are built by sequentially dipping into ZrP and dye-PAH solutions to form

* To whom correspondence should be addressed.

10.1021/jp982086c CCC: $15.00
Published on Web 11/03/1998

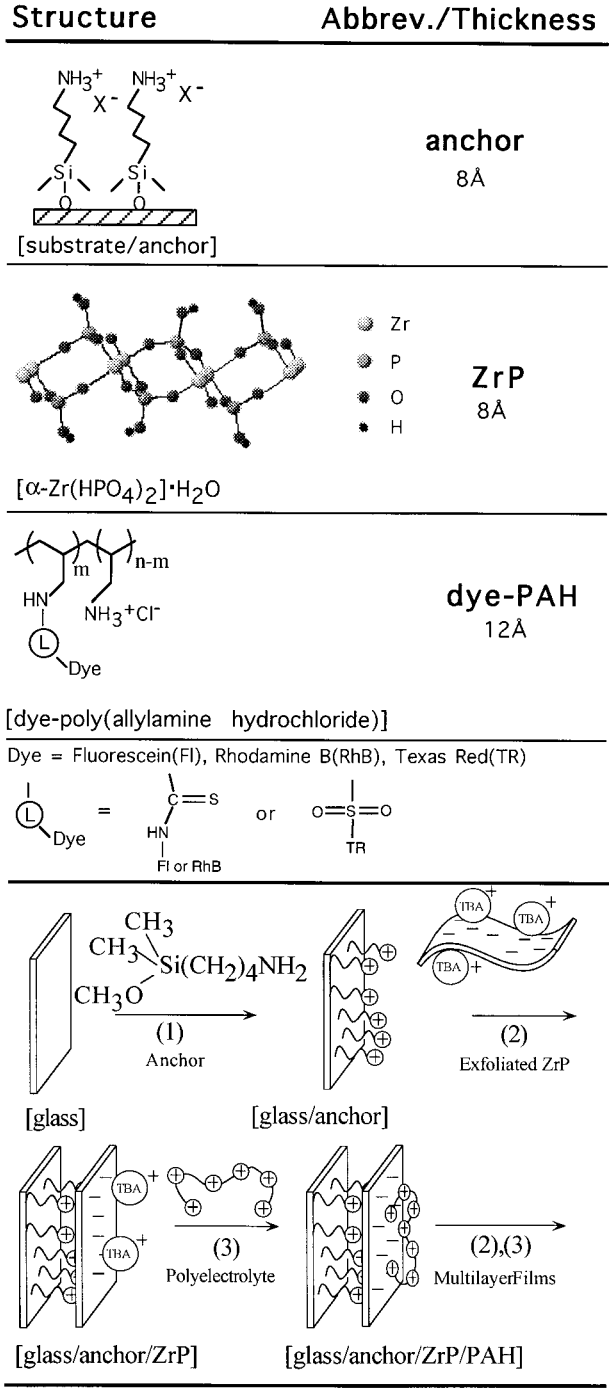

Figure 1. Molecular structures for the component layers of the self-assembled ZrP/dye-PAH multilayer thin films.

the self-assembled structure. The idealized self-assembled ionic structure consists of uniform and flat alternating ionic layers without interlayer penetration.

Fluorescence resonance energy transfer[19−21] between donor and acceptor dye-derivatized polymer layers was previously used as a "spectroscopic ruler" to study the morphology of these self-assembled ionic multilayers.[10] A series of multilayer films were prepared in which the distance between donor ZrP/Fl-PAH and acceptor ZrP/RhB-PAH layers was adjusted by varying the number of intervening nonfluorescent ZrP/PAH layers. In this way, the distance between the chromophores could be adjusted to be smaller or greater than the Förster radius. The energy-transfer efficiencies were calculated from the bulk fluorescence spectra and compared to theoretical efficiencies in order to measure the interlayer penetration and distance separation. The results were consistent with the idealized self-assembled ionic structure.

The present study utilizes the high topographical and optical/spectroscopic resolution of near-field scanning optical spectroscopy (NSOM) in conjunction with AFM to *directly spatially resolve the complex nanoscale morphologies and photophysical properties* of ZrP multilayer films. NSOM is a high-resolution scanning probe technique which provides simultaneous topographical (resolution $\approx$ 10 nm) and optical (resolution $\geq$ 30 nm) images of thin-film materials. It has been used to study a wide range of nanostructured thin-film materials, including locally aggregated conjugated polymer thin films, self-assembled aggregate thin films of fluorescent molecules such as porphyrin wheels and J-aggregate yarns, organic nanocrystals, and organic molecular semiconductor heterojunctions.[22−28] The local concentration, local electronic structure, and local molecular orientation of nanostructured thin films has been effectively probed by near-field optical *spectroscopy* (both transmission and emission in conjunction with polarization techniques) via the local electronic spectra (emission and absorption) of these materials.

In this paper, fluorescence NSOM, in conjunction with AFM and bulk fluorescence spectroscopy are used to investigate the self-assembled morphology of thin-film multilayers of glass/anchor/ZrP/dye-PAH and glass/anchor/ZrP/dye-PAH/ZrP/dye-PAH (where dye = Fluorescein (FL), Rhodamine B (RhB), and/or Texas Red (TR)). The major goals of this paper are to spatially resolve the nanoscale morphology and spectroscopy of the multilayer films. In particular, spatially resolved fluorescence energy-transfer efficiencies are used as a new tool to determine the integrity of the multilayer assemblies.

Experimental Section

Surface Modification. The conditions for the preparation of the self-assembled films have been described elsewhere.[9,10] The ZrP was exfoliated by proton exchange with tetrabutylammonium hydroxide to yield single sheets of ZrP suspended in aqueous solution (7 mM, pH $\approx$ 10.4). The modified substrate was then exposed to the exfoliated ZrP solution to adsorb the single sheets of ZrP onto the surface.

Various functionalized dyes, Fluorescein (FL), Rhodamine B (RhB), and Texas Red (TR), were attached to the polycation PAH. FL-PAH and RhB-PAH were available from another study[10] and TR-PAH was made with a similar reaction. The polymer (PAH, 2×10^{-3} mol) was dissolved in 5 mL of deionized water with 9×10^{-4} mol of sodium bicarbonate. Texas Red (Sulforhodamine 101 acid chloride, 8×10^{-5} mol) was dissolved in 10 mL of DMF at 2° C and added to the PAH solution, mixed thoroughly, and then incubated for 1 h in the dark. The TR−PAH was precipitated from the reaction solution with an excess of acetone.

The dye-PAH layer was adsorbed onto the glass/anchor/ZrP substrate by suspending a few drops of ~10 mM layer solution (at neutral pH) only on one side of the glass coverslip for 10 min. In this way, more layers were produced by repeating the adsorption of the ZrP and dye-PAH solutions. After each adsorption step, the substrate was rinsed with DI water and dried with a stream of argon gas. Dye-PAH layers were also adsorbed onto clean bare glass and amine-derivatized glass coverslips in order to assess the affinity of the polymer for the different substrates.

Optical Spectroscopy. Bulk UV−vis spectra were taken on a diode array HP8452A UV−Vis spectrometer. The fluorescence

spectra were taken on a SPEX Fluorolog 1680 0.22 m double spectrometer using front-face illumination and collection geometry. The bulk fluorescence emission and excitation spectra were corrected for the instrument response.

NSOM Measurements. NSOM measurements were made on a modified Topometrix Aurora near-field microscope using homemade NSOM probes. The apparatus and analogous experimental methods have been described in detail elsewhere.[25−29] Sub-wavelength-resolution probes (typically 50−100 nm resolution) were routinely obtained. The NSOM results were observed to be highly reproducible and not subject to artifacts due to sample heating by the NSOM probe, sample-tip contact, or photolysis of the samples by the near-field excitation.

The self-assembled multilayer films were excited by either the 488 nm line from an Ar^+ ion laser or the 543.5 nm line from a green He−Ne laser. The amount of light coupled into the NSOM probe was always kept below 0.5 mW to limit the amount of "tip heating" on the sample.[30] In a typical experiment, with a 80 nm aperture tip and coupling 150 μW into the NSOM probe, the excitation intensity was extrapolated to be 1.5×10^9 photons/s on the detector side.

In some NSOM experiments, two single-photon-counting avalanche photodiode detectors (APD's) (EG&G Canada SPCM-203-PQ) were used to monitor either two different polarization directions or two different spectral regions. Two optical images were recorded simultaneously, and either a broadband polarizing beam splitter (400−700 nm Melles Griot) or a 50/50 nonpolarizing beam splitter was used. Near-field fluorescence spectra were taken by introducing an additional 50/50 beam splitter into the system. In this case, one-half of the fluorescence was sent to a polychromator (Acton Spectra Pro 150) and the other half to the APD's. The polychromator was equipped with a 300 g/mm grating and a liquid nitrogen cooled CCD (Princeton Instruments, LN/CCD-1024E). Binning of the pixels on the CCD limited the spectral resolution to about 1 nm.

Low excitation levels were used for the near-field fluorescence spectra in order to avoid photobleaching effects. To check that the spectra were not complicated by photobleaching, near-field fluorescence spectra were recorded at various excitation intensities while the sample was scanned and left stationary. The excitation intensity was reduced to a level where consecutive spectra on the same region could be reproduced and showed similar signals. In most experiments, the excitation was about 1×10^9 photons/s and each spectrum was collected for 20 s. These conditions were especially important for the bilayer films since photobleaching affects could potentially alter the energy-transfer efficiency and the fluorescence spectrum. Spectra taken while scanning the sample and while stationary were similar and comparable to the bulk spectra on the monolayer films. Near-field photobleaching of the multilayer films (glass/anchor/ZrP/RhB and glass/anchor/ZrP/TR) did not show a change in the shape of the fluorescence spectra. The same regions on the films were also imaged several times to ensure that there was no change in the topography and optical properties of the sample due to the NSOM tip. In experiments where the sample was purposely photobleached, the excitation intensity was increased to about 5×10^9 photons/s and changes in the fluorescence were then studied. All the NSOM fluorescence spectra were corrected by subtracting a background spectrum obtained on a clean glass cover slip or on a region of the film that was scratched away. The scratched region provided a convenient method to continuously check the background emission from the NSOM probe. The background is usually a broad fluorescence band that is attributed to emission from the single-mode fiber, and in some cases, the NSOM tip may pick up loose objects from the surface which are usually attributed to the dye-PAH material. The background correction is usually not more than 5% and does not significantly alter the spectrum.

TABLE 1: Theoretical and Measured Vertical Heights (Å) of ZrP/R−PAH Multilayered Thin Films

	theor[a]	AFM	shear force	ellipsom[b]
anchor	8	5		8
ZrP	8	13(7)[c]	35(15)	8−10
dye-PAH	∼12			8−12
anchor/ZrP/RhB−PAH	∼28	26(9)[c]	38(19)[d]	22
anchor/ZrP/TR−PAH	∼28		30(15)[d]	
anchor/ZrP/RhB/ZrP/TR	∼48		48(15)[c]	

[a] Estimates from approximate molecular dimensions and/or dimensions from crystal structures. [b] References 9 and 10. [c] Heights obtained from Figure 2a and 2b. [d] Heights obtained from Figure 3.

AFM Measurements. AFM images were obtained with a Digital Instruments Nanoscope IIIA AFM operating in the tapping mode using a 3045JVW piezo tube scanner. The 125 μm etched silicon cantilevers had a resonant frequency between 250 and 350 kHz, and the oscillation frequency for scanning was set to ∼0.1−3 kHz below resonance. Typical images were obtained with line scan rates of 2 Hz while collecting 256 × 256 pixel samples.

Results and Discussion

Nanoscopic Self-Assembled Structure of the Thin Films. AFM images of glass/anchor/ZrP and glass/anchor/ZrP/RhB structures are shown in Figure 2a and b, respectively. ZrP sheets are clearly resolved in the glass/anchor/ZrP image. The ZrP sheets are on average 150 nm in diameter, lie flat on the surface, and form a densely packed "tiled" structure. More than 95% of the surface is covered by the sheets. Presumably regions of glass and/or anchor are exposed in the cracks between the sheets. The root-mean-square (rms) roughness of the film is 1 nm. Adsorption of a polymer overlayer to form the glass/anchor/ZrP/RhB assembly results in a film with a similar topographic character and rms roughness, indicating that the polymer overlayer uniformly conforms to the ZrP sheets. The observed average heights from the AFM image are in good agreement with the theoretical estimates of layer thickness for perfectly packed layers and are listed in Table 1. The polymer appears to adhere predominately to the ZrP sheets, since individual sheets are clearly observed and have heights consistent with an anchor/ZrP/RhB layer.

In some cases, tall sharp features appear at the edges of the ZrP sheets (Figure 2a). These features have heights that range up to ∼ 40 nm. A separate study has assigned the features to zirconium oxide and has shown that they result from hydrolysis of ZrP.[17] Formation can be eliminated by controlling the temperature and pH during ZrP exfoliation. In fact, the multilayer film in Figure 2c was prepared with conditions inhibiting the ZrP hydrolysis and correspondingly shows few of these tall features.

The integrity of the multilayer films is maintained as additional layers are added to the film. The high-resolution shear-force topographic image (obtained with an uncoated NSOM tip) of a glass/anchor/ZrP/RhB/ZrP/TR multilayer assembly is shown in Figure 2c. Plate structures are clearly resolved and cover more than 95% of the surface. Cracks between the upper ZrP sheets reveal the underlying ZrP/RhB sheets, the anchor layer, and/or the bare glass. Step edges are also observable where one ZrP/TR plate stacks on top of an underlying ZrP/RhB plate. The rms roughness of this film is 2

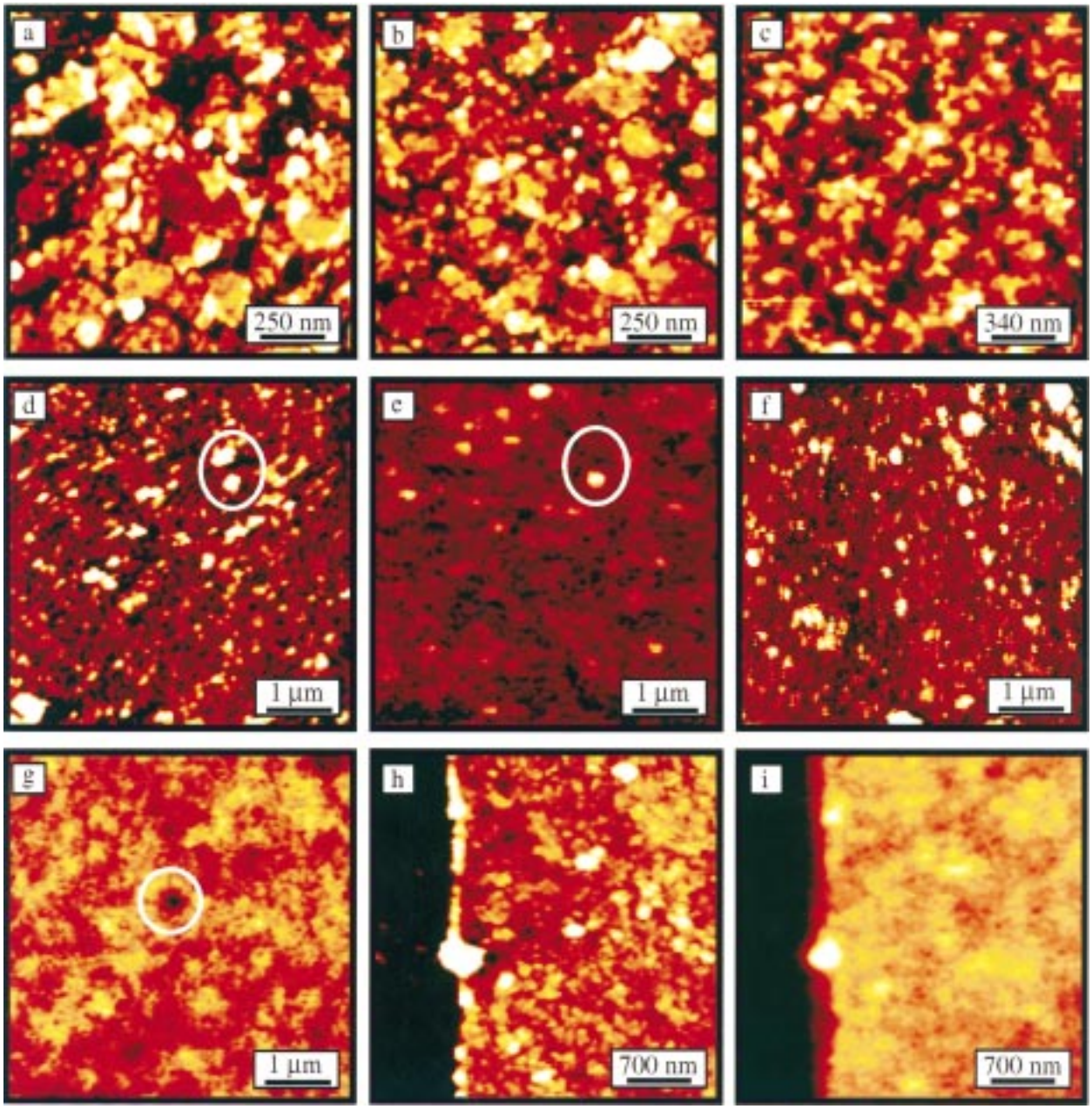

Figure 2. Noncontact AFM image of glass/anchor/ZrP (a) and glass/anchor/ZrP/RhB (b), and shear-force (uncoated fiber) topographical image of glass/anchor/ZrP/RhB/ZrP/TR (c). Topography (d) and the associated near-field fluorescence image (e) of glass/anchor/ZrP/FL. Topography (f) and the fluorescence near-field image (g) of glass/anchor/ZrP/RhB. A 230 nm fwhm photobleached hole is circled in g. Topography (h) and the associated near-field fluorescence image (i) of glass/anchor/ZrP/RhB/ZrP/TR. The sample in h was scratched with an Al-coated NSOM tip.

nm. The height of the ZrP/RhB/ZrP/TR layer assembly, measured from the shear-force image, is 48(15) Å which is in excellent agreement with the theoretical estimate (48 Å).

Topographic and corresponding fluorescence NSOM images of glass/anchor/ZrP/FL, glass/anchor/ZrP/RhB, and glass/anchor/ZrP/RhB/ZrP/TR multilayer films are shown in Figure 2d−i, respectively. Due to the blunt aluminum-coated fiber-optic NSOM probe, the topographic images in Figure 2d, f, and h are less well-resolved than the topographic images in Figure 2a−c as imaged by noncontact AFM and shear force using a sharp uncoated probe. A variability in the topographic resolution is observed between different aluminum-coated NSOM probes, and in general, the tiling is not as well-resolved in densely packed films. In less densely packed films, the coated NSOM probe can resolve individual ZrP sheets (see Figure 3 below). Figure 2 displays representative topographic images of many samples (prepared under similar conditions) that were studied by either noncontact AFM or shear force (uncoated and coated probes).

The fluorescence NSOM image (Figure 2e) of the glass/anchor/ZrP/FL film was obtained by photoexcitation at 488 nm and collection of all fluorescence. The assembly shows weak uniform fluorescence across the film, except for small localized regions of increased emission (Figure 2e, circled area). The tiling is not resolved in the fluorescence image due to a number of factors. Fluorescein films are weakly fluorescent which leads to poor signal-to-noise. Also, the surface may be well tiled and the optical resolution not sufficient to resolve the individual ZrP domains. The fluorescent features in the NSOM image are correlated with ~30 nm high features in the topographic image (Figure 2d) and are assigned to coiled regions of FL-PAH polymer. Fluorescein is negatively charged at pH above 6.5.[31]

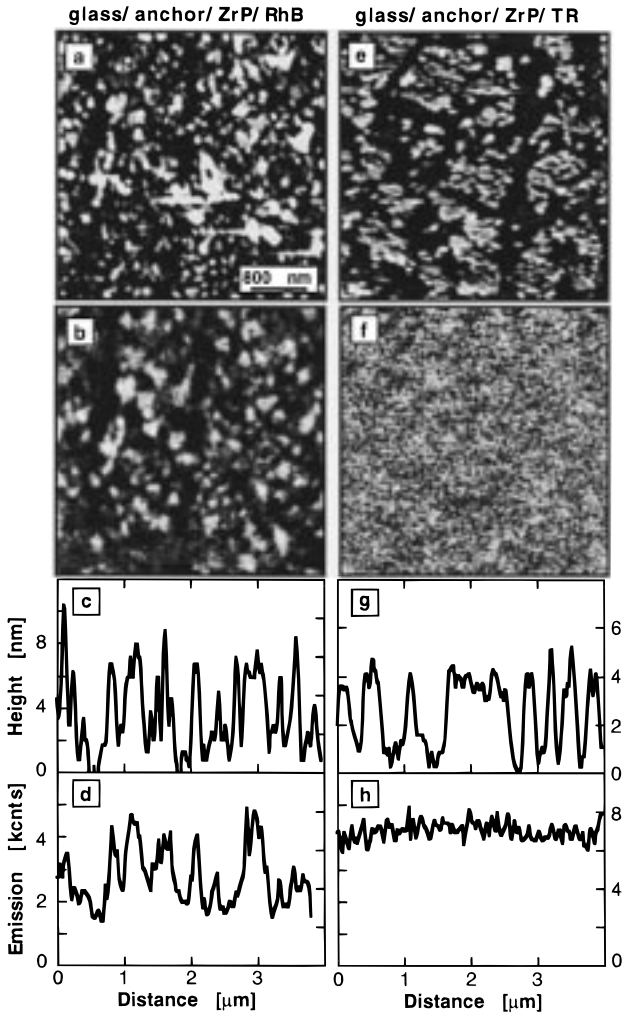

Figure 3. NSOM data of samples displaying incomplete coverage. Left column: Topography (a) and the associated near-field fluorescence (b) image of glass anchor/ZrP/RhB with linescans of the topography (c) and fluorescence (d) image. Right column: Topography (e) and near-field fluorescence (f) image of glass/anchor/ZrP/TR and linescans of the topography (g) and emission (h) images.

Incomplete protonation of the dye-labeled polymer to form the polycationic structure apparently results in intramolecular deprotonation of fluorescein by the residual-free bases of the polymer, resulting in coiling of the polymer.

The topographic and corresponding fluorescence NSOM images of the glass/anchor/ZrP/RhB multilayer system are shown in Figure 2f and g, respectively. The variability in fluorescence intensity in Figure 2g is likely the result of increased RhB−PAH concentration in the regions of ZrP sheets. The average fluorescence intensity over the image area varies by 9%. Although, the tiling is difficult to observe in the printed topographic image (Figure 2f), close analysis of the image on a computer monitor reveals some correlation between surface features (presumably ZrP sheets) and increased RhB−PAH emission. Unfortunately, the quality of printed images can be inferior to the image quality observed on a computer monitor. Therefore, the reader is encouraged to view the images on the World Wide Web version of this manuscript or the TIFF images that have been included in the Supporting Information.

The topographic image (Figure 2f) also reveals tall sharp features ~40 nm in height (without corresponding spikes in the fluorescence) assigned to zirconium oxide as described above in the case of Figure 2a. To demonstrate that the fluorescence NSOM image is due predominantly to the RhB emission, a photobleached dark spot or "hole" was created by parking the NSOM tip locally and photoexciting the sample for an extended period (Figure 2g, circled area). A circular hole measuring 230 nm wide was formed. The topographic image is, however, unchanged by this extended irradiation, verifying that the film is not physically damaged by irradiation or local heating, even for extended periods.

The fluorescence NSOM shows that the integrity of the films is maintained when additional ZrP and dye-PAH layers are adsorbed. The topographical and fluorescence NSOM images of a glass/anchor/ZrP/RhB/ZrP/TR multilayer assembly are shown in Figure 2h and i, respectively. The film was photoexcited at 545 nm, and all emission was collected at the detector. Both RhB and TR absorb substantially at 545 nm, yet the emission spectrum of the multilayer film closely resembles the TR-only spectrum (see below), indicating efficient energy transfer to the upper TR layer. The average fluorescence intensity is 20 kcnts/s over the film area and varies by 10%. Areas of increased fluorescence are correlated with the location of ZrP sheets in the upper layer. The TR−PAH covers the surface of the film. The topographical and NSOM images suggest that the tiling is nearly complete beneath the polymer surface. To establish a "zero level" for the NSOM and topographic images, the film was scratched with an aluminum-coated NSOM probe. The scratched region is seen as the dark region in Figure 2h and i. The extremely weak emission in the scratched region is due to residual dye material and background emission from the fiber.

Fluorescence NSOM imaging with polarized excitation and detection revealed no observable polarization effect. This demonstrates that the chromophores within the polymer layers on the ZrP sheets are not preferentially ordered within the optical spatial resolution of ~50 nm. The fluorescence from the coiled polymer regions shown in Figure 2e was also unpolarized.

In summary, the data indicate that these multilayer films conform well to the idealized picture presented for self-assembled ZrP/polyelectrolyte ionic multilayered assemblies. *The high-resolution NSOM, noncontact AFM, and shear-force measurements show that (i) single sheets of ZrP pack closely and lay flat on the substrate, (ii) the polymer adheres predominately to the surface of the ZrP sheets and fills in the cracks between the sheets to a lesser extent, (iii) the structure of the film is maintained in the multilayer assemblies, (iv) the chromophores within the layers do not show preferential ordering within the optical spatial resolution of ~50 nm.*

Spatially Isolated Self-Assembled Bilayer Islands. The local morphology of defect regions of the multilayered assemblies have been investigated in detail by studying samples with incomplete tiling, i.e., ZrP layers with poor surface coverage. Such samples are occasionally produced by the standard synthetic procedure, perhaps as a result of incomplete formation (silanization) of the anchor layer. The topographical and fluorescence NSOM images of a glass/anchor/ZrP/RhB multilayer film displaying incomplete tiling of the substrate are shown in Figure 3a and b, respectively. Isolated islands of ZrP are clearly resolved in the topographic image. The height of the islands measured from the shear-force topographic image is 38(19) Å and is larger than expected for isolated ZrP sheets (8 Å), which suggests that RhB−PAH has self-assembled on top of the sheets. However, the location of the RhB−PAH polymer cannot be discerned from the topographic image alone. The corresponding fluorescence NSOM image, Figure 3b, clearly reveals that more emission emanates from the regions of the

ZrP sheets. This is dramatically shown in linescan plots taken from the topographic and fluorescence NSOM images. Every peak in the topographic linescan, Figure 3c (the peaks represent the location of the ZrP sheets), is reproduced in the corresponding fluorescence NSOM linescan, Figure 3d (the peaks represent the location of the dye-labeled RhB−PAH). In these multilayer films, the polymer has a higher affinity for the upper surface of the ZrP sheets than for the exposed substrate. The RhB−PAH self-assembles preferentially on the ZrP domains and tends to avoid the spaces between the sheets.

In contrast, the topographic and fluorescence NSOM images of a glass/anchor/ZrP/TR multilayer film with incomplete coverage reveal a much different nanoscale morphology (Figure 3e and f, respectively). Isolated islands of ZrP, which measure 30(15) Å in height and ∼150 nm in diameter, are observed in the shear-force topographic image. However, the corresponding fluorescence NSOM image, Figure 3f, reveals emission from the entire film. There is not a correlation between the location of the islands and the fluorescence. The topographic and NSOM linescans are shown in Figure 3g and h. The fluorescence signal across the film is relatively uniform and varies by only 10%. In this film, the TR−PAH polymer binds equally well to the ZrP sheets and to the exposed substrate.

The affinity of the polymer for bare glass and for anchor-derivatized glass have been further investigated by examining unsilanized and silanized glass substrates which were dipped in a solution of dye-PAH to make glass/dye-PAH and glass/anchor/dye-PAH films (dye = RhB and TR). The NSOM fluorescence images of glass/dye-PAH films (not presented) reveal intense uniform fluorescence with ∼7% variation in the fluorescence intensity over the examined region of the surface. The corresponding topographic images have less than 1 nm variation in height. These data are consistent with the expectation that unsilanized glass, which is neutral to slightly basic, presents a slightly anionic surface which leads to efficient adsorption of the polycationic dye-PAH.

The glass/anchor/dye-PAH films, in contrast, are weakly fluorescent and reveal only small domains of dye emission in the NSOM fluorescence images. The silanized surface, however, is cationic, and consequently, the polycationic dye-PAH polymer is electrostatically repelled and does not adhere well to the surface. The small fluorescent domains seen in the NSOM images are assigned to regions where the polymer readily adsorbs and may correspond to regions of unsilanized glass (i.e., interruption of the anchor layer).

These observations have important implications for interpreting the NSOM images of the multilayers (Figure 3). In particular, for glass/anchor/ZrP/RhB, the decreased concentration of RhB−PAH polymer in the regions between the ZrP islands may be a consequence of a poorly silanized surface and, hence, cationic substrate in these regions. Conversely, the binding of the polycationic TR−PAH polymer to the entire surface in the glass/anchor/ZrP/TR multilayer film suggests that the exposed surface between the islands of ZrP in this film is predominately unsilanized glass.

Spatially Resolved Energy Transfer in Self-Assembled Films. Further insight into the morphology of the multilayer assemblies was obtained by investigating the fluorescence energy-transfer efficiencies in localized regions of the films. The energy-transfer efficiency, in turn, was used to estimate the local effective distance between the donor (RhB) and acceptor (TR) layers. As mentioned above, fluorescence resonance energy transfer can be used to measure donor/acceptor distances in the 10−80 Å range.[32] The energy-transfer efficiency

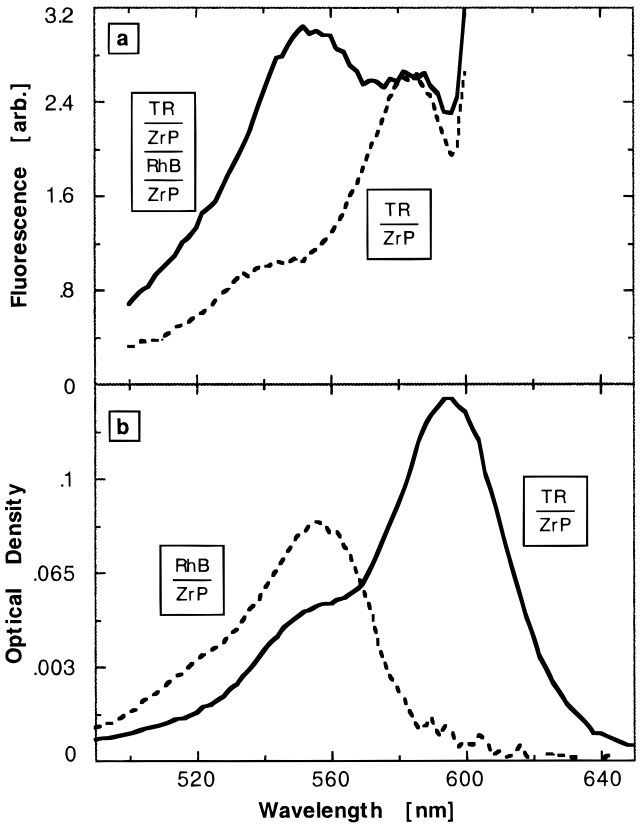

Figure 4. Fluorescence excitation spectra (a), monitored at 610 nm, of glass/anchor/ZrP/TR (- - -) and glass/anchor/ZrP/RhB/ZrP/TR (—). Absorption spectra (b) of glass/anchor/ZrP/RhB (- - -) and glass/anchor/ZrP/TR (—).

E depends on the inverse-sixth-power of the distance R between the donor and the acceptor, as follows

$$E = 1/(1 + [R/R_0]^6)$$

R_0 is the distance at which 50% of the energy is transferred from the donor to the acceptor.

R_0 is a function of various parameters and can be estimated from measurements on the donor and acceptor multilayer films, leading to an estimate of 31 Å for R_0.[33]

The far-field fluorescence excitation spectra (λ_{coll} = 610 nm, TR:Fl_{max} = 610 nm) of glass/anchor/ZrP/TR and glass/anchor/ZrP/RhB/ZrP/TR are shown in Figure 4a. The absorption spectra of films containing 10 layers of RhB and TR are shown in Figure 4b. To record an absorption spectra, multiple dye-tagged polymer layers were necessary. Five layer self-assembled structures were coated on each face of a microscope cover slip to obtain the absorption spectra shown in Figure 4b. The TR multilayer film absorbs slightly more than the RhB film. The excitation spectrum of the glass/anchor/ZrP/RhB/ZrP/TR multilayer film monitored at 610 nm (the emission maximum of the energy acceptor TR) shows two clearly resolved maxima at 553 and 590 nm which correspond to the maxima of the RhB and TR absorptions. The emission spectrum of this film is nearly identical to the emission spectrum of the glass/anchor/ZrP/TR film (see Figure 5a and below). Photoexcitation into the RhB absorption results in energy transfer to TR. The efficiency of energy transfer can be obtained from the excitation spectrum of the energy acceptor (RhB) in the glass/anchor/ZrP/RhB/ZrP/TR multilayer film. The magnitude of the spectrum A at any given wavelength is given by $A = \epsilon_A + E\epsilon_D$, where E is the

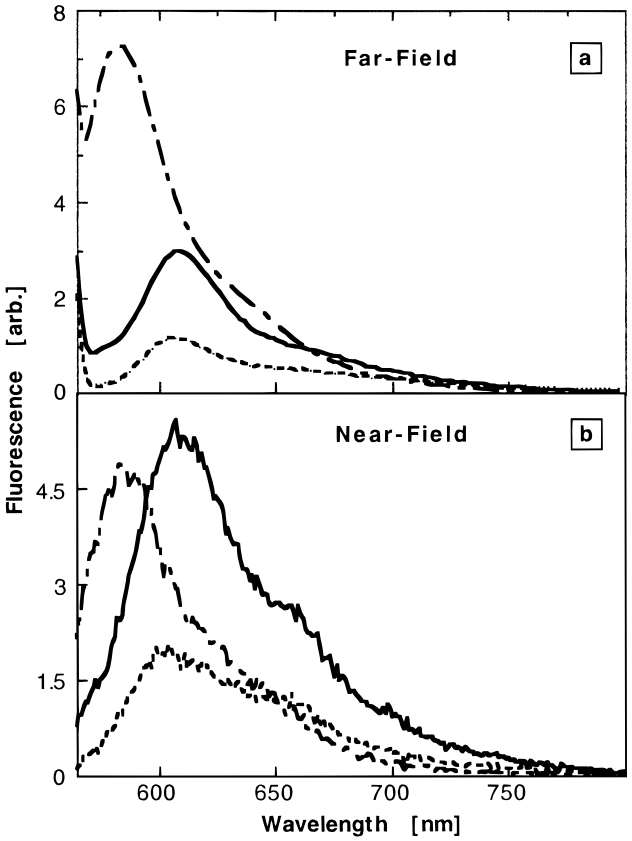

Figure 5. Bulk fluorescence (a) and NSOM fluorescence (b) spectra of the glass/anchor/ZrP/RhB (-—-), glass/anchor/ZrP/TR (- - -), and glass/anchor/ZrP/RhB/ZrP/TR (—) multilayered films. Photoexcitation was at 545 nm for both a and b.

energy-transfer efficiency, ϵ_D is the absorption extinction coefficient of the energy donor, and ϵ_A is that of the acceptor.[19] In the case of energy-transfer efficiencies near unity, the shape of the acceptor fluorescence excitation spectrum will match the shape of the sum of the absorption curves for the donor and the acceptor. The sum of the absorption spectra in Figure 4b results in a curve (not shown) which closely matches the fluorescence excitation curve of the RhB/TR multilayer film. From the excitation curve alone it can be concluded that the energy-transfer efficiency is quite high, approaching unity.

Bulk fluorescence spectra and spatially resolved NSOM fluorescence spectra of the various multilayer films (glass/anchor/ZrP/RhB, glass/anchor/ZrP/TR, and glass/anchor/ZrP/RhB/ZrP/TR) are displayed in Figure 5a and b, respectively. The far-field and near-field spectra (peak positions, shapes, and bandwidths) are similar for both the glass/anchor/ZrP/RhB and glass/anchor/ZrP/TR films. This is consistent with vibronic broadening being the major factor in determining the emission band shape, further suggesting that any additional environmentally induced broadening is fully represented by the number of dye molecules in the excitation volume of the near-field experiment. Interestingly, the ratio of NSOM-induced integrated fluorescence intensities for the glass/anchor/ZrP/RhB vs glass/anchor/ZrP/TR films is a factor of 2 smaller than the same comparison with far-field excitation. This may be due to quenching by the NSOM tip, but we have not explored this effect in detail.

The spatially resolved energy-transfer efficiencies of the glass/anchor/ZrP/RhB/ZrP/TR assembly have been calculated by fitting the fluorescence spectra to a linear combination of the pure RhB and TR spectra in order to estimate the contributions

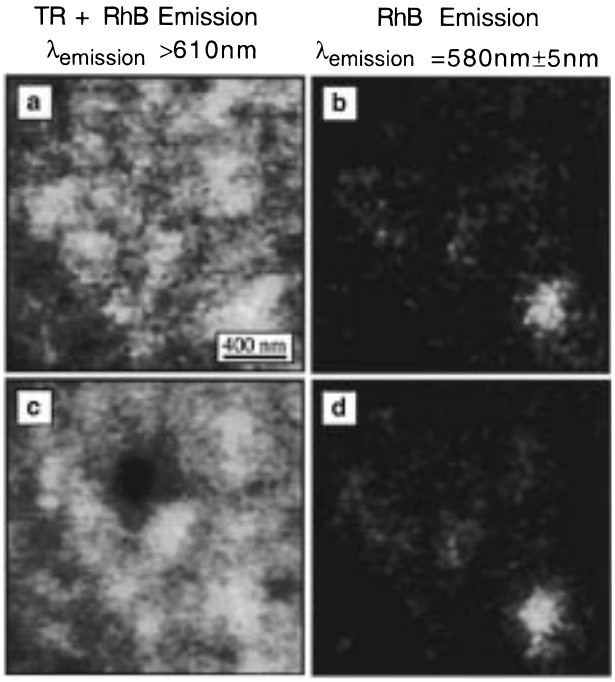

Figure 6. Dual-wavelength fluorescence NSOM images of glass/anchor/ZrP/RhB/ZrP/TR. Fluorescence images a and b were obtained prior to photobleaching. Fluorescence images c and d are of approximately the same region obtained after photobleaching with 545 nm light. Images a and c correspond to emission >610 nm (TR and RhB emission). Images b and d correspond to fluorescence at 580 ± 5 nm (predominately RhB emission).

of the two components.[10,32] The average energy-transfer efficiency measured from the *bulk far-field* fluorescence data is 0.91, corresponding to a 21 Å separation between the layers. This is in close agreement with the theoretical estimate of $E = 0.93$ for randomly oriented RhB and TR dye layers separated by 20 Å, where $R_0 = 31$ Å. Near-field fluorescence measurements in ~50 nm spatially isolated regions of the sample indicate, on average, 0.93 energy-transfer efficiency in the film corresponding to a 20 Å separation. Small site to site variations in the near-field fluorescence spectra were observed. Energy-transfer efficiencies as large as 1.0 and as small as 0.83 were also identified. The variations in energy-transfer efficiency by ±0.1 is consistent with small variations in the average D−A separation of ca. ±4 Å. Our measurements cannot distinguish effectively between interpenetration from distances of 16 Å to near contact, since such distances would result in energy-transfer efficiencies near unity. Energy-transfer dye pairs with $R_0 = 10$ Å would be more suited to spectrally follow the details of interpenetration of closely spaced dye layers separated by single ZrP spacers. D−A distances greater than ~24 Å would result in efficiencies less than 83% but are not observed in these multilayer films. Spatially resolved NSOM fluorescence spectra show that the energy-transfer efficiency in these multilayer films is generally high with an average E of 0.93 ± 0.10 obtained from the NSOM measurements, corresponding to a 20 ± 4 Å separation between the dye layers. These data support the idealized structural model of the self-assembled ionic layers.

Dual wavelength NSOM spectral imaging of the glass/anchor/ZrP/RhB/ZrP/TR multilayer film was performed in order to spatially resolve the energy-transfer efficiency and uniformity of the films on the nanoscopic length scale (Figure 6a and b). In these experiments, two different detectors monitored different spectral regions. A 580 ± 5 nm interference filter was placed prior to one detector in order to predominately monitor the RhB

fluorescence (RhB, Fl_{max} = 580 nm; TR, high-energy edge of the emission band). A 610 nm long-pass filter was placed in front of the other detector to predominately monitor TR emission and to a lesser extent the RhB emission (TR, Fl_{max} = 610 nm; RhB, >610 nm = low-energy tail of the emission band). The 580 and >610 nm images show variations in the emission intensity of 28% and 12%, respectively, indicating fairly uniform coverage of the polymer films in the plane of the substrate. The fluorescence intensity in the 580 nm image is substantially less than that observed at >610 nm due to the narrow spectral window and weak fluorescence from RhB (efficient energy transfer to TR). Local intensity variations in the fluorescence image are often correlated with local features in the topographical image (not shown). *In regions where the upper surface shows the signature of ZrP sheets, brighter fluorescence spots are observed in both fluorescence images*. Increased self-assembly of the polycationic TR−PAH polymer layer is expected to occur at the polyanionic ZrP sheets. Furthermore, the upper ZrP sheets are likely to have been adsorbed onto locations where there was higher concentrations of the polycationic RhB−PAH polymer. *Self-assembly of ionic multilayers is more likely to occur at the sites where the electrostatic interactions are highly favorable.* Much of the substrate reveals the densely tiled structure of ZrP plates (see Figures 2c, h, i and 6a,b). Much of the surface is well-characterized by the idealized self-assembled structure of ionic multilayer films. In these regions where the upper-layer ZrP sheets are observable in the topographic image, it is likely that the average donor−acceptor separation is at least 20 Å, since the dye layers are separated by an impenetrable ZrP plate. Increased emission from the RhB underlayer is expected in these regions since the dye layers are separated by a fixed distance and energy-transfer efficiency is on the order 0.93. At the edges of sheets and in the cracks between the sheets, greater interpenetration and little if any emission from the donor RhB is expected to occur.

Distinct features of interpenetration in the glass/anchor/ZrP/RhB/ZrP/TR assembly were spatially resolved with dual-wavelength fluorescence NSOM. These features are relatively rare in these multilayer films. The topographical and the corresponding 580 and >610 nm fluorescence images of a 40 nm high feature are shown in Figure 7a−c, respectively. The 580 nm NSOM image shows a bright region (indicating the presence of RhB) which is correlated with the topographic feature. The island is not composed of a fully derivatized coil of polymer since the fluorescence intensity is quite small for the measured height. The fluorescence intensity is comparable to a single layer of the RhB polymer. The fluorescence spectra of the feature and the surrounding area are shown in Figure 8a. The fluorescence from the surrounding area closely resembles the TR spectrum and is likely the result of extensive energy transfer from RhB to TR in the closely separated layers. The fluorescence spectrum of the 40 nm feature, however, is intermediate between RhB and TR and contains approximately equal contributions from both chromophores. However, there is very little energy transfer between the chromophores in the feature since the fluorescence intensities monitored at 580 and >610 nm decrease at the same rate upon photobleaching with 545 nm light. If there was energy transfer, a rise in the 580 nm emission intensity at early times would be expected (see below). The chromophores associated with the feature are separated by distances greater than the Förster radius. The feature could potentially be a coil of polymer with a small loading of chromophores or a polymer-coated feature (dust particle or hydrolyzed ZrP).

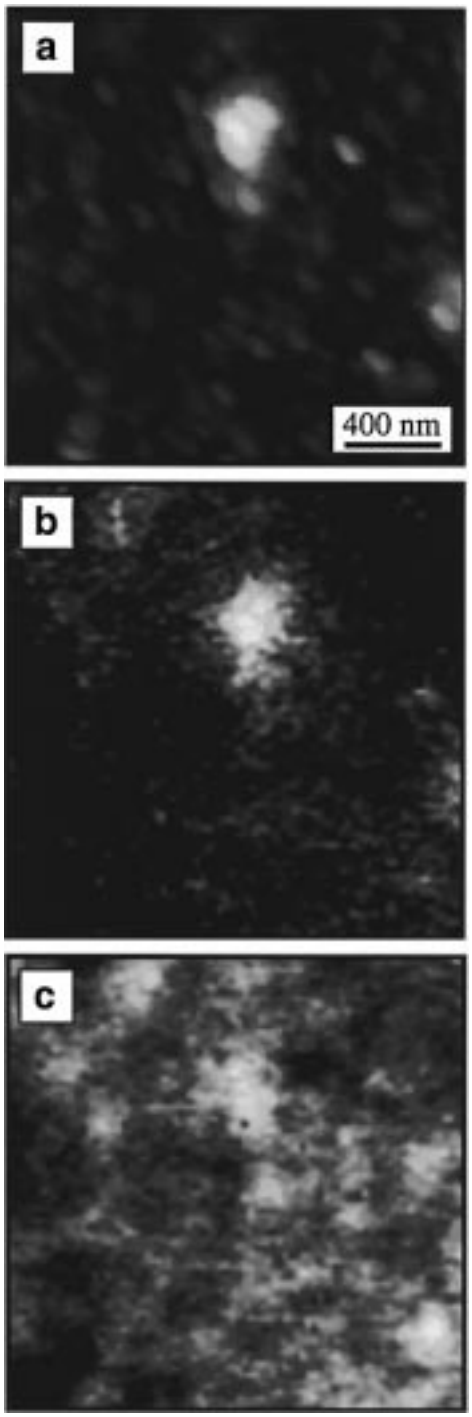

Figure 7. Topographical (a) and corresponding NSOM fluorescence b and c images of a glass/anchor/ZrP/RhB/ZrP/TR assembly. Images b and c were collected in different spectral regions. Image b monitors the RhB emission at 580 ± 5 nm, and c monitors all emission >610 nm and, therefore, contains emission from both RhB and TR.

Identifying Energy Transfer Domains by Photobleaching. This section is concerned with applications of near-field photobleaching experiments to study the spatial distribution of energy-transfer efficiencies and the spatial distribution of donor and acceptor concentrations. The experiments entailed the positioning of the near-field tip over an area of interest and locally photoexciting the sample to photochemically "bleach" both of the dye−polymer layers. Bleaching was performed with 545 nm excitation, where both chromophores absorb. Separate experiments on glass/anchor/ZrP/RhB and glass/anchor/ZrP/TR demonstrated that the photobleaching efficiency of the TR and

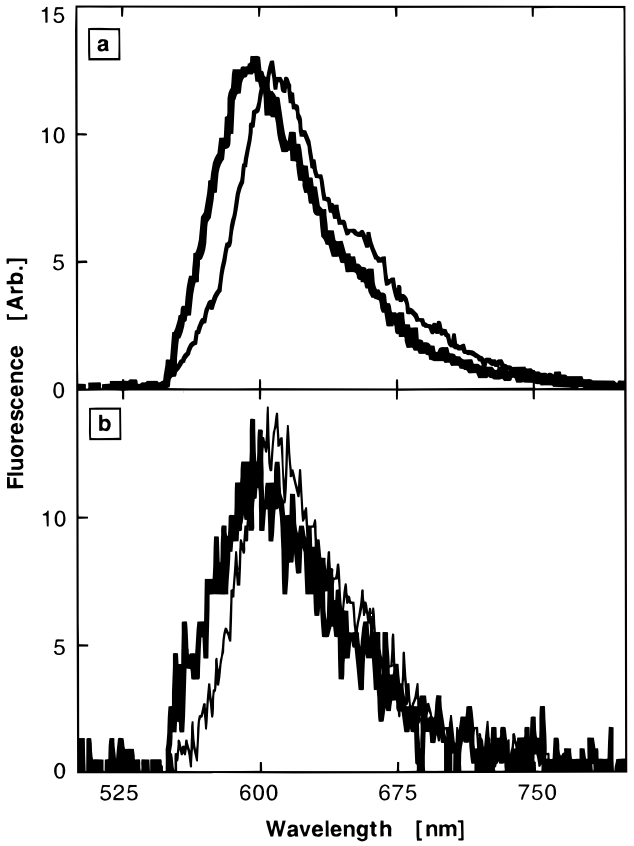

Figure 8. (a) Normalized NSOM fluorescence spectra taken on the "brighter" region (thick line) and the surrounding "darker" region (thin line) in fluorescence image Figure 7b. (b) NSOM fluorescence spectra of glass/ZrP/RhB/ZrP/TR prior to (thin line) and after (thick line) photobleaching with 545 nm light.

RhB chromophores are comparable at this wavelength. Dual-wavelength NSOM spectral images of the glass/anchor/ZrP/RhB/ZrP/TR multilayer before and after photobleaching a hole using 545 nm are shown in Figure 6. The photobleached area is readily visible as the dark hole in the >610 nm fluorescence image, Figure 6c. There are no observable topographical changes caused by the photobleaching process. The bleached hole in the >610 nm emission image shows a 60% reduction in fluorescence intensity. The 580 nm fluorescence image (RhB emission, Figure 6d) appears nearly unchanged. The near-field fluorescence spectra obtained prior to and after photobleaching of the film reveal a blue shift in the fluorescence (Figure 8b). Figure 9 displays the fluorescence intensities as a function of irradiation time for the 580 and >610 nm spectral region which were monitored simultaneously during the photobleaching of the hole. The signal-to-noise ratio in the 580 nm kinetic trace is less than the >610 nm kinetic trace due to the narrow band of emission collected at 580 ± 5 nm. The 580 nm RhB emission initially increases by 30% and then slowly decays back to its initial value. The >610 nm emission (RhB and TR) shows a decay of 60% due to photobleaching. The initial rise in the 580 nm emission (increased emission of the donor RhB) at early photobleach times is direct evidence of energy transfer in this local region of the multilayer assembly. At early photobleach times, energy is efficiently "funneled" from RhB to TR, causing the TR to bleach faster. As the TR is bleached, the energy transfer deactivation channel of RhB fluorescence is removed and consequently an increase in the RhB fluorescence is observed. At longer photobleach times, the observed bleach kinetics become comparable in both spectral windows.

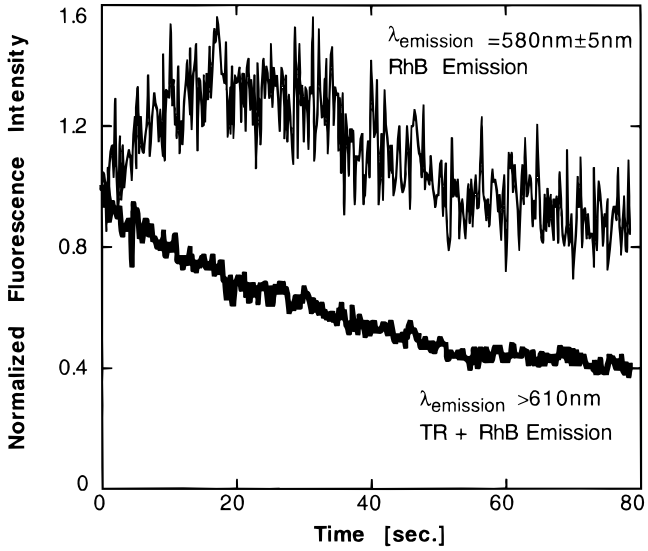

Figure 9. Fluorescence intensity in the 580 nm and >610 nm spectral windows recorded as a function of time. The kinetic traces were recorded during the photobleaching of glass/anchor/ZrP/RhB/ZrP/TR with 545 nm light. The photobleached hole is shown in Figure 6. An initial increase in the RhB emission (580 ± 5 nm) is observed as the TR is photobleached. The emission at 580 ± 5 nm (thin line) and >610 nm (thick line) are shown.

Domains that display little or no energy transfer between donor and acceptor chromophores have also been identified. For example, the NSOM fluorescence spectrum of the tall feature in Figure 7 contains contributions from RhB and TR. Near-field photobleaching of this feature with 545 nm light shows that the fluorescence decay kinetics monitored in the 580 and >610 nm spectral windows are identical and that there is no initial increase in the RhB emission. Thus, the D−A chromophores are separated by distances greater than the Förster radius.

Conclusions

Spectrally and spatially resolved NSOM has been used to investigate the complex nanoscale morphologies, fluorescence energy-transfer efficiencies, and spectroscopy of self-assembled ZrP/ionic multilayer films. The high-resolution spectroscopic and topographic measurements demonstrate that the films self-assemble in accordance with the simple idealized picture of such assemblies: *single* sheets of ZrP lay flat on the substrate and pack closely, "tiling" the surface. The polymer adheres predominately to the ZrP sheets and fills in the cracks between the sheets to a lesser extent. The structure of the film is maintained as additional layers of ZrP/R-PAH are adsorbed. The chromophores within the layers do not show preferential ordering within the optical spatial resolution of ∼50 nm. Furthermore, the chemical sensitivity of NSOM has allowed for a determination of the morphology of defect regions, which include hydrolyzed ZrP features, incomplete tiling of ZrP sheets, and local regions of coiled polymers. Finally, spatially resolved NSOM fluorescence spectra and photobleaching studies have shown that the energy-transfer efficiency is extremely high (0.93) over most of the sample. This corresponds to a ∼20 ± 4 Å average separation between the chromophores within the layers.

Acknowledgment. The research at Minnesota was supported by the National Science Foundation. Work at Penn State was supported by the Division of Chemical Sciences, Office of Basic

Energy Sciences, Department of Energy, under Contract No. DE-FG02-93ER14374

Supporting Information Available: Electronic TIFF files of all of the images in this paper. See any current masthead page for Internet access instructions.

References and Notes

(1) Lehn, J. M. *Supramolecular Chemistry*; VCH Publishers: Weinheim, 1995.

(2) Whitesides, G. M.; Simanek, E. E.; Mathias, J. P.; Seto, C. T.; Chin, D. N.; Mammen, M.; Gordon, D. M. *Acc. Chem. Res.* **1995**, *28*, 37.

(3) Decher, G. *Science* **1997**, *277*, 1232.

(4) Desiraju, G. R. *Angew. Chem., Int. Ed. Engl.* **1995**, *34*, 2311.

(5) Cao, G.; Hong, H.; Mallouk, T. E. *Acc. Chem. Res.* **1992**, *25*, 420.

(6) *Supramolecular Architecture*; Bein, T., Ed.; American Chemical Society: Washington, DC, 1992.

(7) Marks, T. J.; Ratner, M. A. *Angew. Chem., Int. Ed. Engl.* **1995**, *34*, 155.

(8) *Templating, Self-Assembly and Self-Organization*; Sauvage, J. P., Hoseini, M. W., Eds.; Pergamon: Oxford, 1996; Vol. 9.

(9) Keller, S. W.; Kim, H.; Mallouk, T. E. *J. Am. Chem. Soc.* **1994**, *116*, 8817.

(10) Kaschak, D. M.; Mallouk, T. E. *J. Am. Chem. Soc.* **1996**, *118*, 4222.

(11) Torgerson, M. R.; Nocera, D. G. *J. Am. Chem. Soc.* **1996**, *118*, 8739.

(12) Bideau, J. L.; Papoutsakis, D.; Jackson, J. E.; Nocera, D. G. *J. Am. Chem. Soc.* **1997**, *119*, 1313.

(13) Byrd, H.; Suponeva, E. P.; Bocarsly, A. B.; Thompson, M. E. *Nature* **1996**, *380*, 610.

(14) Vermeulen, L. A.; Snover, J. L.; Sapochak, L. S.; Thompson, M. E. *J. Am. Chem. Soc.* **1993**, *115*, 11767.

(15) Byrd, H.; Snover, J. L.; Thompson, M. E. *Langmuir* **1995**, *11*, 4449.

(16) Snover, J. L.; Byrd, H.; Suponeva, E. P.; Vicenzi, E.; Thompson, M. E. *Chem. Mater.* **1996**, *8*, 1490.

(17) Kaschak, D. M.; Johnson, S. A.; Kim, H. N.; Mallouk, T. E. Manuscript in preparation.

(18) Kim, H. N.; Keller, S. W.; Mallouk, T. E.; Schmitt, J.; Decher, G. *Chem. Mater.* **1997**, *9*, 1414.

(19) Stryer, L.; Haughland, R. P. *Proc. Nat. Acad. Sci.* **1967**, *58*, 719.

(20) Latt, S. A.; Cheung, H. T.; Blout, E. R. *J. Am. Chem. Soc.* **1965**, *87*, 995.

(21) Kuhn, H.; Möbius, D. *Angew. Chem., Int. Ed. Engl.* **1971**, *9*, 620.

(22) Hofkens, J.; Latterini, L.; Vanoppen, P.; Faes, H.; Jeuris, K.; Defeyter, S.; Kerimo, J.; Barbara, P. F.; Deschryver, F. C.; Rowan, A. E.; Nolte, R. J. M. *J. Phys. Chem.* **1997**, *101*, 10588.

(23) Vanden Bout, D. A.; Kerimo, J.; Higgins, D. A.; Barbara, P. F. *Acc. Chem. Res.* **1997**, *30*, 204.

(24) Adams, D. M.; Kerimo, J.; Olson, E. J. C.; Zaban, A.; Gregg, B. A.; Barbara, P. F. *J. Am. Chem. Soc.* **1997**, *119*, 10608.

(25) Vanden Bout, D. A.; Kerimo, J.; Higgins, D. A.; Barbara, P. F. *J. Phys. Chem.* **1996**, *100*, 11843.

(26) Higgins, D. A.; Vanden Bout, D. A.; Kerimo, J.; Barbara, P. F. *J. Phys. Chem.* **1996**, *100*, 13794.

(27) Higgins, D. A.; Kerimo, J.; Vanden Bout, D. A.; Barbara, P. F. *J. Am. Chem. Soc.* **1996**, *118*, 4049.

(28) Reid, P. J.; Higgins, D. A.; Barbara, P. F. *J. Phys. Chem.* **1996**, *100*, 3892.

(29) Betzig, E.; Trautman, J. K. *Science* **1992**, *257*, 189.

(30) La Rosa, A. H.; Yakobson, B. I.; Hallen, H. D. *Appl. Phys. Lett.* **1995**, *67*, 2597.

(31) Sjöback, R.; Nygren, J.; Kubista, M. *Spectrochim. Acta Rev.* **1995**, *51*, L7.

(32) Ha, T.; Enderle, T.; Ogletree, D. F.; Chemla, D. S.; Selvin, P. R.; Weiss, S. *Proc. Nat. Acad. Sci.* **1996**, *93*, 6264.

(33) R_0 can be estimated from $R_0 = [(8.79 \times 10^{-5})J(\lambda)\phi_D n^{-4}\kappa^2]^{1/6}$ [Å] where $J(\lambda)$ is the overlap integral between the normalized donor fluorescence and the acceptor absorption scaled by the extinction coefficient, ϕ_D is the quantum yield of fluorescence of the donor, n is the refractive index of the medium, and κ^2 is a geometrical factor which accounts for the orientation of the two dipoles. For the RhB donor and TR acceptor pair, $R_0 = 31$ Å, where $\phi_D = 0.81$, $\kappa^2 = 0.67$ (randomly oriented chromophores), $n = 1.5$, and $J = 1 \times 10^{14}\ M^{-1}\ cm^{-1}\ nm^4$. The energy-transfer efficiency is sensitive to D−A distances near R_0. The estimated average D−A separation in the glass/anchor/ZrP/RhB/ZrP/TR system is 20 Å (thickness of a ZrP layer and a monolayer of randomly oriented polymer). The theoretical energy-transfer efficiency at $R = 20$ Å with $R_0 = 31$ Å is 0.93 for this system. The theoretical energy-transfer efficiencies at $R = 16$, 20, 24, and 31 Å are 0.98, 0.93, 0.83, and 0.5, respectively.